Folate-Conjugated Iron Oxide Nanoparticles for Solid Tumor Targeting as Potential Specific Magnetic Hyperthermia Mediators: Synthesis, Physicochemical Characterization, and in Vitro Experiments

Fabio Sonvico,[†,‡,||] Stéphane Mornet,[§] Sébastien Vasseur,[§] Catherine Dubernet,[†] Danielle Jaillard,[⊥] Jeril Degrouard,[⊥] Johan Hoebeke,[+] Etienne Duguet,[§] Paolo Colombo,[‡] and Patrick Couvreur*[,†]

UMR CNRS 8612 Physico-chimie, Pharmacotechnie, Biopharmacie - Université de Paris-Sud, Châtenay-Malabry, France, Dipartimento Farmaceutico - Università degli Studi di Parma, Parma, Italy, UPR CNRS 9048 Institut de Chimie de la Matière Condensée de Bordeaux, Université Bordeaux-1, France, National Institute for the Physics of the Matter, Parma, Italy, UMR CNRS 8080 Développement et Evolution - Centre Commun de Microscopie Electronique, Université de Paris Sud, Orsay, France, and UPR CNRS 9021 Immunologie et Chimie Thérapeutiques, Université de Strasbourg, Strasbourg, France. Received February 24, 2005; Revised Manuscript Received July 28, 2005

New folate-conjugated superparamagnetic maghemite nanoparticles have been synthesized for the intracellular hyperthermia treatment of solid tumors. These ultradispersed nanosystems have been characterized for their physicochemical properties and tumor cell targeting ability, facilitated by surface modification with folic acid. Preliminary experiments of nanoparticles heating under the influence of an alternating magnetic field at 108 kHz have been also performed. The nanoparticle size, surface charge, and colloidal stability have been assessed in various conditions of ionic strength and pH. The ability of these folate "decorated" maghemite nanoparticles to recognize the folate receptor has been investigated both by surface plasmon resonance and in folate receptor expressing cell lines, using radiolabeled folic acid in competitive binding experiments. The specificity of nanoparticle cellular uptake has been further investigated by transmission electron microscopy after incubation of these nanoparticles in the presence of three cell lines with differing folate receptor expression levels. Qualitative and quantitative determinations of both folate nanoparticles and nontargeted control nanoparticles demonstrated a specific cell internalization of the folate superparamagnetic nanoparticles.

INTRODUCTION

In recent years, colloidal carriers have elicited many hopes for their potential as vectors for therapeutics and diagnostics in cancer therapy (*1*, *2*). As reviewed recently, metal-based colloids have many interesting applications in the biomedical field, too (*3*, *4*). For example, iron oxide nanoparticles, prospected in diagnostic clinical practice as magnetic resonance imaging enhancers in the mid 80s and currently in clinical phase IV, are nowadays among the most successful application of nanotechnologies in medicine (*5*, *6*). Nevertheless, some decades ago, such particles were already suggested as a tool to manage hyperthermia in solid tumors by heating them with alternating magnetic fields (*7*). Hyperthermia treatment of tumor and metastasis has, indeed, been demonstrated to be effective, either alone, the neoplastic cells being more thermosensitive than the normal ones, or in association with classical chemo- or radiotherapies (*8*–*10*). Despite some preliminary interesting results in preclinical tumor animal models (*11*), hyperthermia using superparamagnetic iron oxide particles has, however, been overlooked for almost a decade. Thanks to a new wave of interest for this technique, since the early 90s, a lot of progress has been made, especially in the field of superparamagnetic materials, so that finally the time seems to be ripe for the start of clinical studies (*12*, *13*). The hyperthermia is obtained by applying an alternating magnetic field of suitable frequency that produces heat dissipation through the oscillation of the internal magnetic moment of the superparamagnetic particles (*14*). Among the developments that have been considered for nanoparticle-mediated hyperthermia, we have focused our attention on the opportunity to achieve an intracellular hyperthermia treatment (*15*). The interest lies in the specific delivery of heat to target cells causing selective damage to their cytoplasm structures. Recently, a very similar approach, in which laser-absorbing gold nanoparticles were used, has been successfully applied to obtain specific targeting and killing of cancer cells (*16*). In the present study, we describe a new type of dextran-coated maghemite superparamagnetic nanoparticles targeted toward solid tumors through folate, covalently bound to the nanoparticle surface using a poly(ethylene)-

* To whom correspondence should be addressed. Université de Paris XI - Centre d'études pharmaceutiques, 5, rue J.B Clément, 92296 Châtenay-Malabry, France. Phone: +33-(0)1-46835396. Fax: +33-(0)1-46619334. E-mail: Patrick.couvreur@cep.u-psud.fr.

† UMR CNRS 8612 Physico-chimie, Pharmacotechnie, Biopharmacie - Université de Paris-Sud.

‡ Università degli Studi di Parma.

§ Université Bordeaux-1.

|| National Institute for the Physics of the Matter.

⊥ UMR CNRS 8080 Développement et Evolution - Centre Commun de Microscopie Electronique, Université de Paris Sud.

+ Université de Strasbourg.

10.1021/bc050050z CCC: $30.25
Published on Web 09/02/2005

glycol (PEG) spacer. Folic acid (FA) has been chosen as the targeting moiety, since it has been observed that many solid tumors, such as ovarian and breast cancers, overexpress the specific receptor for this vitamin. In this paper, these FA-conjugated superparamagnetic nanoparticles have been characterized for their physicochemical properties, their heating capacity, and their efficacy in targeting cancer cells overexpressing the folate receptor.

MATERIALS AND METHODS

All chemicals and reagents, except where indicated, were provided by SIGMA-Aldrich (St.Quentin Fallavier, France). Cell culture media and reagents were obtained from Invitrogen-Lifetechnologies (Cergy Pontoise, France).

Superparamagnetic Nanoparticles Preparation. *Dextran-Coated Maghemite Nanocrystals Production.* Dextran-coated superparamagnetic maghemite (γ-Fe_2O_3) nanocrystals have been produced through a procedure already described (*14*, *15*). Briefly, the cores were produced by the coprecipitation of Fe(III) and Fe(II) ions in alkaline conditions, oxidation, and peptization to obtain a maghemite (γ-Fe_2O_3) cationic ferrofluid as previously reported (*16*). Subsequently, the surface modification of crystals was carried out by adding an amino silane coupling agent, γ-(aminopropyl)triethoxysilane, in methanol/water medium (1:1), followed by thermal treatment at 100−110 °C in glycerol for 2 h under vacuum. The flocculated particles were then washed with acetone and water and peptized with nitric acid until pH = 3. Such a ferrofluid was stable in a pH range of 1 to 8. The magnetic nanoparticles were sterically stabilized by activated dextran (70 kD). The activation was performed by partial oxidization of dextran vicinal diols into aldehyde groups with sodium metaperiodate. The oxidized dextran was allowed to react with the amino groups of maghemite in order to be anchored through covalent imine bonds (Shiff's bases). The colloidal suspension was washed by tangential ultrafiltration against 3 L of ultrapure water with a poly(ethersulfone) membrane (cutoff 100 000 g/mol) and stored at room temperature. Such dextran-coated maghemite nanoparticles may be described as a new covalent platform useful for MRI contrast enhancement as well as hyperthermia mediators. They were called VUSPIO for versatile ultrasmall superparamagnetic iron oxide (*14*, *15*).

Folate Conjugation. N-Hydroxysuccinimide ester of FA (NHS-folate) was prepared according to a method previously described (*17*). Briefly, 5 g of FA, dissolved in 100 mL of dry dimethyl sulfoxide containing 2.5 mL of triethylamine, was reacted with 2.6 g of *N*-hydroxysuccinimide in the presence of 4.7 g of dicyclohexylcarbodiimide overnight at room temperature. After removing the byproduct (dicyclohexylurea) by filtration, the yellow solid NHS-folate was then extracted by precipitation in diethyl ether, washed several times with anhydrous ether, and dried under vacuum. Amino−PEG−folate was prepared as follows: 1.351 g of NHS-folate was dissolved in 50 mL of DMSO and slowly added to 250 mL of carbonate/bicarbonate buffer (1 M, pH 11 adjusted with HCl 37%) containing 5 g of diaminotelechelic−PEG (Jeffamine ED-2003 from Huntsman, Salt Lake City). Two hours later, the solution was dialyzed against 5 L of water (MwCo 1000 g/mol). The dialysis procedure was repeated every 24 h for a total of 5 times. Amino−PEG−folate was characterized by ^{1}H NMR (300 MHz, DMSO-d_6): δ 8.61 (s, 7-H of FA, 1H), 7.65 (d, 13,15-H of FA, 2H), 6.64 (d, 12,16-H of FA, 2H), 4.25−4.15 (m, 19-H of FA, 1H), 3.75−3.45 (m, CH_2CH_2 of PEG, ∼170H), 1.07−0.87 (m, propylene CH_3 Jeffamine ED-2003, ∼15H). UV analysis allowed the determination of the folate content in the final product: 26.3 mg of amino−PEG−FA were dissolved in 2 mL of 10 mM phosphate buffer, 0.15 M NaCl, pH 7.5, diluted 50 times in phosphate buffer and analyzed by UV. The folate content was estimated on the basis of the FA extinction coefficient $\epsilon_M = 6197\ M^{-1}\cdot cm^{-1}$ at 363 nm and found equal to the average value of 1.02 folate group per amino−PEG−FA macromolecule.

Maghemite nanoparticles coated with activated dextran were then reacted with 75 mol % of monoamino−PEG and 25% of amino−PEG−FA in a 0.1 M borate buffer pH 9 in the presence of sodium borohydride 0.206 M. The pH was maintained at pH 9 by adding dropplets of NaOH 0.1 M. When the pH value was stabilized, the solution was left to react for 4 h at room temperature. In such conditions, the generated Schiff's bases were stabilized by reductive amination (VUSPIO−PEG−FA). The excess of unreacted materials and borate salts were removed through tangential ultrafiltration. The control nanoparticles were prepared according to the same procedure with 100% of monoamino−PEG (VUSPIO−PEG).

Physicochemical Characterization of Nanoparticles. *Nanoparticles Size and Surface Charge.* The mean particle size was determined by dynamic light scattering (DLS, N4Plus, Beckman-Coulter, USA). Hydrodynamic diameter measurements were performed at 20 °C and 90° angle, after dilution of the sample to 150 μg/mL iron oxide concentration either in NaCl solutions of increasing concentrations (up to 1 M), or in 0.01 M phosphate buffers at various pH (ranging from 4 to 10). Each sample was analyzed six times for a total period of analysis of 20 min. The surface charge of the nanoparticles was investigated through ζ potential measurements (Zetasizer 4, Malvern Instruments, UK) after dilution of the samples in 0.01 M phosphate buffers at pH between 4 and 10. Smoluchowsky approximation was applied in the calculation of ζ potential.

Nanoparticle Density. The density of the nanoparticles in suspension was measured at 20 °C using a high-precision digital densitometer (Analyzer Beer 2, Anton Paar, Austria). The densitometer was standardized using air (0.001238 g/cm^3) and water (0.998314 g/cm^3) at the same temperature. The nanoparticle density was calculated, as previously described (*21*), by successive approximation from the nanoparticles concentration and the density values obtained for the suspension and for the suspending medium (MilliQ water adjusted at pH 7.4 with NaOH), assuming that no interaction occurred between the nanoparticles and the suspending fluid.

Nanoparticle Structure and Morphology. The morphology of the nanoparticles was investigated by transmission electron microscopy (TEM, EM208 Philips, The Netherlands, operating at 80 keV) and high-resolution TEM (JEOL 2010, JEOL, Japan, operating at 200 keV) observations. Colloid suspensions were deposited on UV-ionized copper grids coated with Formvar film (200 mesh). After 5 min, the excess suspension was removed and the samples were observed. Electron diffraction experiments on samples prepared in the same way, but with nickel grids, have been performed in order to confirm the presence of the iron oxide crystals in the nanoparticles (CM 12, Philips, Netherlands).

Nanoparticle Heating. Magnetic heating of aqueous suspensions of nanoparticles (in the concentration range 2.5−3 $g_{maghemite}$/L) were performed under an alternating field of H_{max} = 88 mT and ν = 108 kHz, produced by a

Celes inductor C97104. Temperature was monitored by alcohol thermometer to avoid any inductive or capacitive heating of the temperature probe. The specific absorption rate was calculated using the simplified relation

$$SAR = \frac{C_{\text{water}}}{x_{\text{Fe}}} \frac{\Delta T}{\Delta t}$$

where C_{water} is the specific heat capacity of water, x_{Fe} is the mass fraction of iron, and $\Delta T/\Delta t$ is the slope of the temperature vs time dependence.

Targeting Properties of the Folate-Conjugated Nanoparticles. *Surface Plasmon Resonance Measurements.* Surface plasmon resonance was used to investigate the efficacy of the interaction between the FA binding protein (FBP) and the folate-functionalized nanoparticles. Measurements were carried out using a BIAcore 3000 (Pharmacia Biosensor AB, Sweden). Cows milk FBP was immobilized onto the surface of a carboximethyldextran-coated gold film (Sensor chip CM-5, BIAcore, Sweden) by amine coupling performed according to the general procedure recommended by the BIAcore supplier (*22*). Briefly, the flow channel of BIAcore was equilibrated with Hepes buffered saline (HBS = 10 mM Hepes pH 7.4, 150 mM NaCl, 3 mM EDTA, 0.005% surfactant P20), and then the following samples were successively injected into the system: (a) *N*-hydroxysuccinimmide solution + *N*′-(3-dimethyl-amino-propyl)-*N*-ethylcarbodiimide solution (1/1, v/v) to activate the carboxylated-dextran surface; (b) 1 mg/mL of FBP in 100 mM phosphate buffer pH 7.0, 4 mM mercaptoethanol, 10% v/v glycerol, and (c) 1 M ethanolamine pH 8.5, to quench residual *N*-hydroxysuccinimidyl esters on the sensor chip. FBP immobilization was then carried out afterward using a flow rate of 5 μL/min. Nanoparticle suspensions in HBS (1.07 mg/mL of Fe) were injected into the BIAcore flow channel at a flow rate of 5 μL/min and allowed to interact with the immobilized receptor for 10 min. The specific interaction with the protein shifted the wavelength at which the surface plasmon resonance occurred. This shift was registered as response units (RU). In a subsequent experiment of binding, a competitive inhibition was performed, nanoparticles being injected under the above operative conditions in the presence of 4 mM free FA.

In Vitro Cell Culture Experiments. *Cell Culture.* The cells cultivated for in vitro experiments were human epithelial mouth carcinoma, KB 3-1 (gift of Dr. S. Chevillard, Fontenay-aux-Roses, France), human breast adenocarcinoma, MCF7 (ATCC, USA), and human cervix adenocarcinoma, HeLa cell line (gift of Prof. C. Malvy, Institut Gustave Roussy, Paris, France). All cell lines were grown in folate-free Dulbecco Modified Eagle's Medium (FFDMEM) with 10% fetal calf serum, 100 units/mL penicillin and 100 μg/mL streptomycin, 4 mM L-glutamine at 37 °C in a 5% CO_2/95% air humidified atmosphere. The concentration of FA was 5−6 nM in folate-free medium containing serum, therefore close to the natural physiologic conditions (5−30 nM) (*23*, *24*). Cells were grown in the above-mentioned conditions at least 1 week prior the experiments to reach the maximal expression level of the folate receptor (FR) for KB and HeLa cells as described in a previous study (*25*). MCF7 cells, which do not express the FR, were used as control.

Cytotoxicity. Nanoparticle cytotoxicity was assessed by the 3-(4,5-dimethylthiazol)-2-diphenyltertrazolium bromide (MTT) test (*26*). Cells were seeded in 96-well tissue culture plates at a density of 5×10^4 cells/well. After 24 h, the culture medium was replaced with 200 μL of FFDMEM containing increasing concentrations of nanoparticles. After 3 h incubation, 20 μL of a solution of MTT (5 mg/mL in NaCl 0.9%) was added to each well and a further 3 h incubation at 37 °C was allowed. At the end of this time the supernatant was carefully removed from each well, without taking off the blue formazan crystals produced by viable cells. Then to completely dissolve the crystals, 200 μL of solvent (1:1, dimethylformamide/sodium dodecylsulfate 20% aqueous solution) were added to each well followed by 3 h incubation at 37 °C. Colorimetric measurements were performed at 570 nm with a scanning multiwell spectrometer (Multiskan MS, Labsystems, Finland). Absorbance values for untreated wells were taken as control reference (100% survival).

Inhibition of the Uptake of Radiolabeled FA into Cells by Nanoparticles. The interaction of nanoparticles with cells expressing the folate receptors was assessed through the measurement of the inhibition of the free tritium-labeled FA uptake ([^{3}H]-FA), as has been shown previously (*27*). Briefly, KB 3-1 cells were allowed to grow in folate-free medium for 1 week. Thereafter, 5×10^5 cells were seeded in 6-well plates. Wells containing medium but without cells were used as control for the unspecific adsorption of the radiolabeled FA on plastic surfaces. Twenty-four hours later, after careful washing with phosphate-buffered saline (PBS), cells were incubated for 30 min at 37 °C with 1 mL of FFDMEM containing 0.1 μM radiolabeled FA and increasing amounts of FA-functionalized iron oxide particles. Afterward, the plates were rinsed twice with PBS, pH 7.4 at 4 °C. Cells were then treated overnight at ambient temperature with 1 mL of 0.1% v/v Triton ×100, and the amount of radioactivity present in the cell lysate was determined by liquid scintillation counting (LS6000 TA, Beckman-Coulter, USA). The results were expressed as percentage of cell-associated radioactivity, the amount found in the absence of nanoparticles being taken as the 100% uptake value. Experiments were repeated in the same conditions but using control nanoparticles (VUSPIO−PEG). All experiments were replicated at least three times.

Folate-Targeted Nanoparticles Cell Uptake Experiments. The cell uptake of γ-Fe_2O_3 nanoparticles was investigated using TEM. Samples were prepared by the following procedure (*28*): cells grown for 1 week in FFDMEM were incubated for 3 h with nanoparticles (150 μg/mL of γ-Fe_2O_3 in FFDMEM). Then, after repeated washing with PBS, pH 7.4, cells were fixed with 2.5% glutaraldehyde in 0.1 M cacodylate buffer (5 mM $CaCl_2$, 5 mM $MgCl_2$, 0.1 M sucrose, pH 7.2) for 1 h at 4 °C. Samples were postfixed in 1% osmium tetroxide in the same buffer for 1 h at room temperature and washed. Cells were scraped and concentrated in 2.5% agar in 0.05 M cacodylate buffer. The specimens were then treated with 2% uranyl acetate solution for 1 h. The material was subsequently dehydrated by means of ethanol/water solutions, with increasing ethanol content and embedded in a epoxy resin (Epikote 812, Fluka, Switzerland). The samples were cut at 70 nm (ultrathin sections) with an ultramicrotome (Ultracut UCT, Leica, Austria). Ultrathin sections of the preparation were stained with 5% uranyl acetate and Reynolds reagent (0.2% lead citrate) and observed on a transmission electron microscope at 80 kV (EM 208, Philips, Netherlands)

Ultrathin sections (70 nm) of the preparation were obtained and rapidly double stained with 5% uranyl acetate, followed by Reynolds reagent (0.2% lead citrate). The presence of iron oxide nanocrystals within the cells

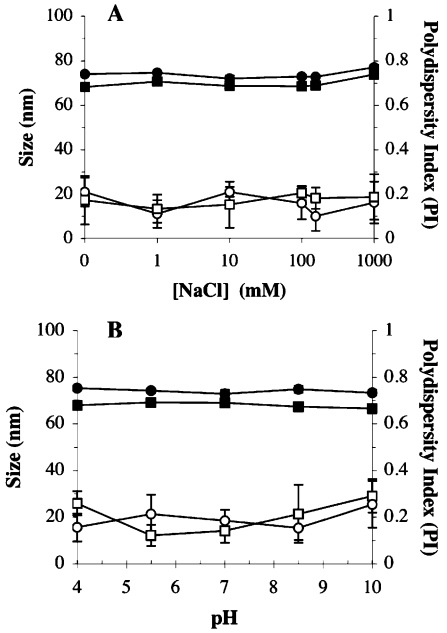

Figure 1. Influence of NaCl concentration (A) and pH (B) of dispersion medium on the hydrodynamic diameter (solid symbols) and polydispersity index (empty symbols) of iron oxide nanoparticles functionalized with PEG (●, ○) and with PEG−FA (■, □). $n = 6 \pm$ standard deviation (SD).

has been confirmed by energy-dispersive X-ray (EDX) spectroscopy and by dark-field observations in TEM (CM12, Philips, The Netherlands, equipped with an EDAX−EDX analyzer). Qualitative and quantitative determination of nanoparticle uptake were obtained by visual localization and counting of the nanoparticles on 10 cell sections for each sample. For each of the three different cell lines a specific uptake index (SUI) was determined and calculated as the ratio between the number of folate-targeted nanoparticles taken up by the cells and the number of nontargeted particles taken up in the same conditions (i.e., nonspecific uptake).

To approximately evaluate the iron oxide concentration achievable within lysosomes, where targeted cells appear to be gathered, an image analysis has been performed using the software ImageJ 1.32j (Wayne Rasband, National Institute of Health, USA). The area of the entire lysosome presented in Figure 9 and the number of particles enclosed have been evaluated. The minimum and maximum values used for detecting particles were 10 and 100 pixels. With the knowledge that the slice observed is 70 nm thick and making the limiting approximation that we see only iron oxide nanocrystals of 5 nm diameter and of known density (4.87 g/cm^3 as calculated for maghemite crystals), we can calculate the iron oxide concentration.

RESULTS

Nanoparticle Size and Surface Charge. As shown in Figure 1, iron oxide nanoparticles, functionalized with PEG or with PEG−FA had a mean diameter between 60 and 80 nm and polydispersity indexes lower than 0.3. pH and ionic strength did not influence significantly either the mean size or the polydispersity index of the nanoparticles. ζ potential measurements showed slight negative values for dextran-coated iron oxide nanoparticles before pegylation (Figure 2). When these nanoparticles were functionalized with PEG, their ζ potential was not affected by the pH of the dispersing medium. On the contrary, when coated with folate-derivatized PEG, the nanoparticle charge got increasingly negative with rising pH which is probably due to the progressive deprotonation of the FA carboxylic groups.

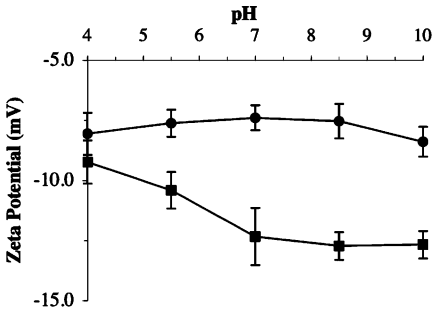

Figure 2. ζ potential values of iron oxide nanoparticles (●, VUSPIO−PEG; ■, VUSPIO−PEG−FA) dispersed in 0.01 M phosphate buffer with pH values between 4 and 10. $n = 10 \pm$ SD.

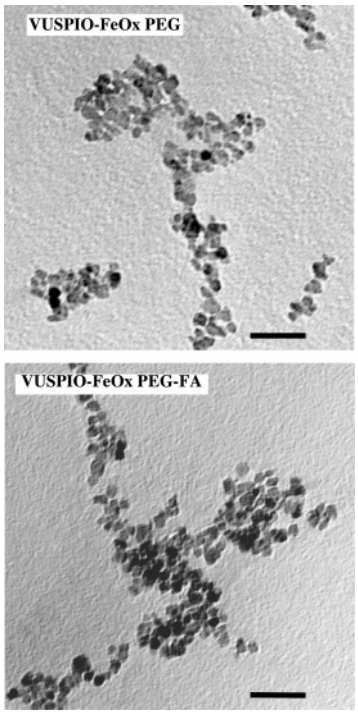

Figure 3. TEM images of PEG−FA and PEG-modified dextran-coated iron oxide nanoparticles (Bar = 50 nm).

Nanoparticle Morphology and Density. As observed by TEM, iron oxide nanoparticles were roughly round shaped with narrow size distribution (Figure 3). Furthermore, it was possible to identify more electron-dense structures nonhomogeneously distributed in their bodies. Their crystalline nature was showed by high-resolution microscopy, while their electron diffraction pattern identified them as maghemite (γ-Fe_2O_3) nanocrystals (Figure 4). The overall particle diameter was between 10 and 20 nm, while the embedded nanocrystals were between 5 and 10 nm. The observed "grapelike" organization of the particles in TEM micrographs is a consequence of the removal of the dispersing phase during sample preparation and is not representative of the real state of nanoparticles in suspension. The difference in the mean sizes obtained by PCS measurements, and electron microscopy has already been observed with other materials (*29*), possibly due to the hydrophilic polymer coating of the particles which increases significantly the hydrodynamic diameter, especially with very

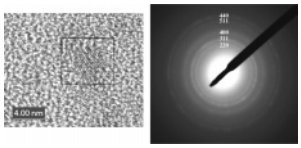

Figure 4. High-resolution TEM image of dextran-coated iron oxide nanoparticle (left). Electron diffraction pattern obtained with the particles, which matches with the one expected for γ-Fe_2O_3 crystals (right).

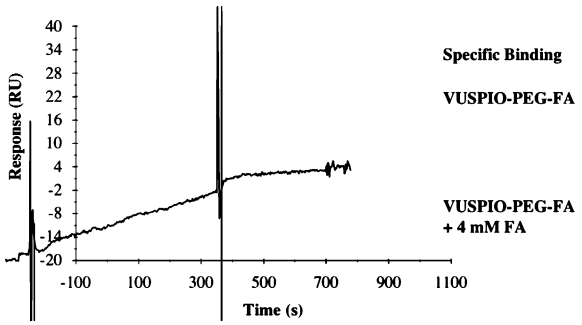

Figure 5. Surface plasmon resonance sensorgram of iron oxide nanoparticles functionalized with PEG−FA (VUSPIO−PEG−FA) and of the same nanoparticles in the presence of 4 mM free FA (VUSPIO−PEG−FA + 4 mM FA). Subtraction of the sensogram in the presence of folate from that in absence of folate gives the specific binding of the nanoparticles to FBP.

small colloids. However, a slight aggregation of nanoparticles in suspension could not be excluded.

The nanoparticle density was found to be 2.76 g/cm^3 due to the presence of high-density nanocrystals (4.87 g/cm^3, as calculated for maghemite crystals). Thus, the number of nanocrystals embedded in individual nanoparticles could be calculated, from the concentration and the density for both of them. The values obtained for different sized nanoparticles varied from 1 to 8 crystals for nanoparticles with diameters between 10 and 20 nm, which is comparable with the TEM observations.

Nanoparticle Heating. Experiments performed on pegylated and folate-conjugated nanoparticles dispersed in water led to quite similar results, with a heating ramp of 7 ± 1 °C per 20 min period. The specific absorption rate, defined as the heating power of the magnetic material per gram, was calculated: SAR = 13 ± 3 W/g_{Fe}. These results are coherent with the ones obtained for the maghemite nanocrystals alone (SAR = 13.8 W/g_{Fe}).

Nanoparticle Cytotoxicity. Both pegylated and folate-linked nanoparticles were tested for their cytotoxicity on three cell lines (HeLa, KB, MCF7) at various concentrations up to 200 μg/mL of Fe_2O_3 (see Supporting Information). After 3 h of incubation only slight cytotoxicity was observed, survival rates being higher than 75% even at the higher nanoparticles concentrations (*30*). Furthermore, no significant difference was shown between the cytotoxicities of the targeted and nontargeted particles (unpaired two-tailed t-test, $p > 0.20$).

Folate Targeting Efficiency. The interaction of the folate-conjugated nanoparticles with the FBP was observed by surface plasmon resonance. In Figure 5, it can be observed that, at the time of sample injection, the addition of a solution having a different refractive index compared to the eluent induced a spike in the signal (RU). The subsequent and progressive increase of the response signal for the folate-conjugated nanoparticles was a sign of the progressive binding of these nanoparticles to the protein linked onto the chip surface. During the washing procedure following the interaction

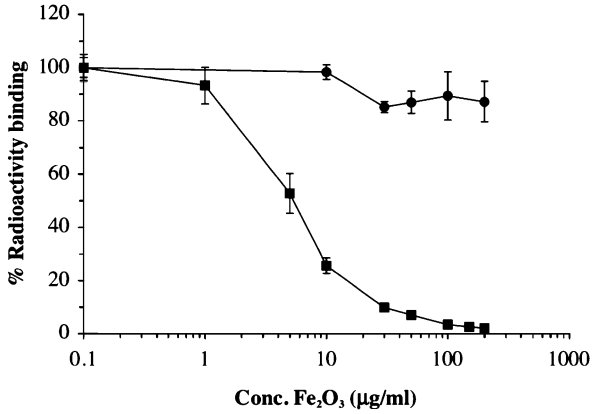

Figure 6. Commpetitive inhibition of the uptake of tritium labeled FA in the presence of increasing concentrations of iron oxide nanoparticles functionalized with PEG−FA (■, VUSPIO−PEG−FA) or PEG alone (●, VUSPIO−PEG). $n = 3 \pm$ SD.

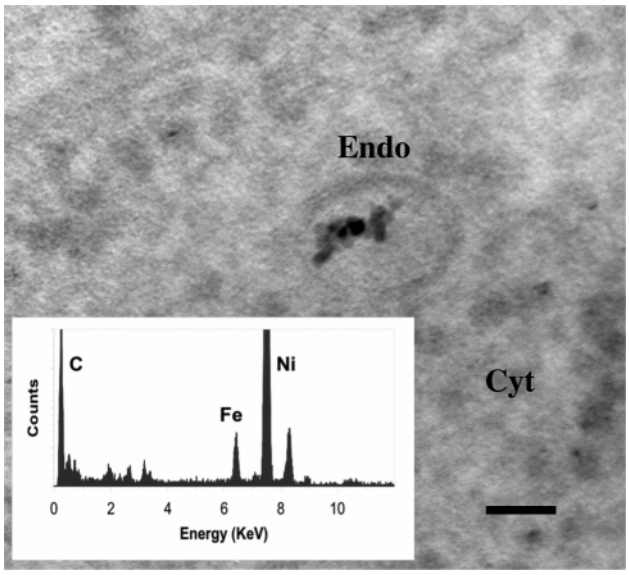

Figure 7. TEM image of an of an agglomerate of few nanoparticles in an endosome in KB cells. The EDX analysis of the object is reported superimposed. (C = carbon; Fe = iron; Ni = nickel; Cyt = cytoplasm; E = endosome; bar = 50 nm).

phase, only a very slight decrease in the signal could be observed, demonstrating a strong specific interaction between the nanoparticles and the FBP. When the experiment was carried out in the presence of free FA (4 mM), no positive signal could be recorded, indicating that the interaction between the folate-functionalized nanoparticles and the chip surface was competitively inhibited by FA free in solution. In control experiments performed with dextran-coated iron oxide nanoparticles functionalized with PEG, no signal was elicited.

To ascertain whether specific interactions between folate-functionalized maghemite nanoparticles and the folate receptor also occurred in vitro, in cell culture conditions, further experiments with tritium-labeled FA were carried out with the KB cell line, which expresses the folate receptor at a dramatically high level (Figure 6). When incubated with radiolabeled FA alone, KB cells avidly captured the radioactive compound. Conversely, FA uptake progressively decreased along with the addition of increasing amounts of folate-targeted nanoparticles (VUSPIO−PEG−FA). It is noteworthy that, for the higher nanoparticle concentrations, almost no cell-associated radioactivity could be detected. Finally, if control nanoparticles (VUSPIO−PEG) were incubated in

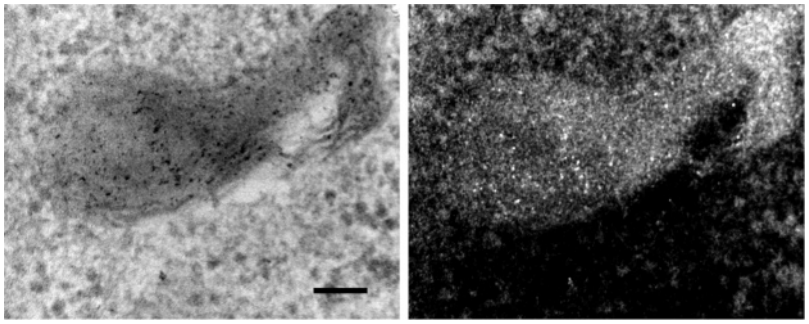

Figure 8. A classic (left) and a dark-field TEM image (right) of a lysosome in KB cells. The electron-diffracting maghemite crystals appear as bright spot in the right image.

Table 1. Uptake of Iron Oxide Nanoparticles by Cells

	nanoparticles taken up per cell[a]		
cell line	VUSPIO−PEG	VUSPIO−PEG-FA	t-test probability
HeLa	15.4 ± 6.9	46.3 ± 18.6	<0.05
KB 3-1	45.2 ± 8.5	307.5 ± 69.7	<0.01
MCF7	58.4 ± 38.3	65.7 ± 60.0	>0.2

[a] Data are presented as mean ± SD (n = 10).

the same conditions, almost no inhibition of the radioactivity cell uptake was observed.

Cell Uptake of Nanoparticles. The uptake of nanoparticles by the different cell lines was investigated by TEM. The presence of iron particles in the intracellular compartment could clearly be identified by EDX spectroscopy, as shown in Figure 7. Maghemite nanocrystals were also recognized by dark-field TEM observations. In these experiments the orientation of the sample was set in order to collect electrons predominantly diffracted by maghemite nanocrystals. Images of KB cell lysosomes containing several nanocrystals are shown in Figure 8.

As predicted from the cytotoxicity experiments, TEM observations showed that cellular structures were well preserved with no visible abnormalities, following incubation with the nanoparticles. In the case of HeLa and KB cells, folate-conjugated nanoparticles were found intracellularly, mainly in endosomes and, especially, in several large multivesicular structures, identified as late endolysosomes, also called residual bodies (see Figure 8). In MCF7 cells, which do not express the folate receptor, we found some nanoparticles near the cell plasmatic membranes and a small number of them were found in lysosomal structures too. Incubation of the three cell lines with control iron oxide nanoparticles without FA bound onto their surface (VUSPIO−PEG) was performed under the same conditions to evaluate the nonspecific cell uptake. The mean number of particles found per cell was calculated for targeted and nontargeted superparamagnetic nanoparticles for each cell line. These results along with a statistical evaluation of their differences (unpaired two-tailed t-test) are presented in Table 1. The targeting efficacy of the folate nanoparticles has been expressed using the SUI, calculated as the ratio between the number of folate-targeted nanoparticles taken up by the cells and the number of nontargeted particles taken up in the same conditions (i.e., unspecific uptake) (Figure 9). In the case of the folate receptor expressing KB and HeLa cells, nanoparticle uptake was greater for targeted nanoparticles (VUSPIO−PEG−FA); the SUI value was approximately 7 (for KB cells) and 3 (for HeLa cells). Conversely, MCF7 cell uptake level of targeted and control particles was quite similar, the SUI being nearly equal to 1. Folate-targeted nanoparticles appeared to be gathered into numerous lysosomes. To determine if the quantity of nanocrystals taken up by cells would be

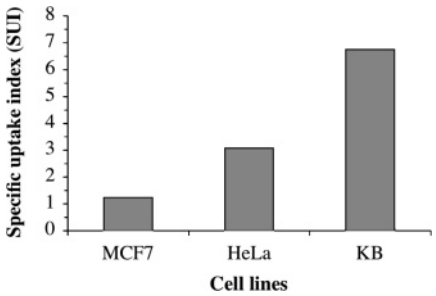

Figure 9. Specific uptake index for the three cell lines. The index is calculated as the ratio between the number of folate-targeted particles (VUSPIO−PEG−FA) internalized by cells and the number of control particles (VUSPIO−PEG) captured by cells in the same conditions.

sufficient for an efficient and rapid heating, we evaluated their concentration in those cellular structures. We calculated that the concentration of iron oxide attained in the endolysosome presented in Figure 8 was in the order of 3 mg/mL.

DISCUSSION

The design of superparamagnetic iron oxide nanoparticles interacting with tumors has received increasing interest in the past few years, as indicated by the number of papers recently published on this subject (*31*−*33*). In particular, the challenge has been to obtain nanoparticles stable in physiological conditions, able to selectively target tumor cells. We produced here iron oxide nanocrystals coated with dextran and successively modified at their surface with PEG and FA. Despite the relatively low surface charge of these nanoparticles, a good colloidal stability has been obtained at both acid and alkaline pH, as well as in the presence of high salt concentrations. This suggests that stabilization of maghemite nanoparticles was primarily dependent on steric repulsion due to their coating with hydrophilic polymers. Thus, dextran and PEG covalently bound to the particle surface are efficient in avoiding their aggregation in the tested conditions, which opens the way for their use in still more complex biological media. These characteristics of stability and steric repulsion should allow these small particles to circulate for a prolonged time in the blood compartment, avoiding the scavenging of the macrophages of the reticulo-endothelial system (*34*, *35*) and allowing the diffusion toward the tumor site, by virtue of the known enhanced permeability and retention effect (*36*, *37*). Furthermore, their superparamagnetic properties were shown not to be modified by the surface functionalization, and particles were able to increase the temperature of an aqueous suspension at a constant rate under an appropriate oscillating magnetic field. With regard to the targeting efficacy, the set of experiments performed in

this study, with plasmon resonance, cell culture competitive assays, and cell nanoparticle capture have clearly demonstrated the capacity of these folate functionalized nanoparticles to specifically target cancer cells with membrane expression of the FA receptor. In fact, as shown in Table 1, the MCF7 cells, deprived of FA receptors, did not uptake more folate-functionalized nanoparticles than the control nanoparticles (no significant difference between the two uptake). In the same conditions, in HeLa and KB cells the folate nanoparticles were taken up in much greater number than the control nanoparticles (significant difference, $p < 0.05$ and $p < 0.01$ respectively). The receptor-mediated endocytotic process ended in the accumulation of the nanoparticles in one of the common metabolic degradation pathways of foreign materials taken up by cells. In fact, the accumulation of folate-targeted molecular conjugates in lysosomes has already been observed with antifolate drugs and folate-targeted carriers such as polyplexes and cyclodextrines (*27*, *38*, *39*). Interestingly, the increase of nanoparticle uptake appeared to be proportional to the folate receptor expression level in HeLa and KB cells. Indeed, as reported before, the folate receptor was 3−4 times more expressed in KB cells compared to HeLa cells (*25*). In addition, the iron concentration attained in cellular structure as lysosomes (3 g/L) appeared to be well suited to obtain a local intracellular heating. Temperature increase to values above 43 °C for a sufficient period of time should be able to cause selective damage and death of cells containing high amounts of iron oxide nanoparticles (*9*).

CONCLUSIONS

In a scientific panorama in which folate-mediated solid tumor targeting seems to become one of the major breakthrough in tumor diagnosis and treatment, the new targeted maghemite nanoparticles presented here are very promising nanosystems for performing a targeted intracellular hyperthermic treatment of tumors overexpressing the folate receptor. Our current research efforts consist in building a hyperthermia apparatus equipped with a large solenoid in which magnetic alternating current field will be homogeneous at the Petri dish scale. Then, in vitro heating experiments will be envisaged and their therapeutic effect will be evaluated.

ACKNOWLEDGMENT

The excellent assistance of Mme. Odile Kaitasov in electron microscopy experiments and of M. Richard Harvey in text reviewing are gratefully acknowledged. Authors would like to thank the Association pour la Recherche sur le Cancer for the financial support to the work of F.S.

Supporting Information Available: Graphs reporting the cytotoxicity of toward HeLa, KB 3-1, and MCF7 cells. This material is available free of charge via the Internet at http://pubs.acs.org/BC.

LITERATURE CITED

(1) Davis, S. S. (1997) Biomedical applications of nanotechnology—implications for drug targeting and gene therapy. *Trends Biotechnol. 15*, 217−224.

(2) Brigger, I., Dubernet, C., and Couvreur, P. (2002) Nanoparticles in cancer therapy and diagnosis. *Adv. Drug Del. Rev. 54*, 631−651.

(3) Sonvico, F., Dubernet, C., Colombo, P., and Couvreur, P. Metallic based nanotechnology, applications in diagnosis and therapeutics. *Curr. Pharm. Des. 11*, 2091−2105.

(4) Mornet, S., Vasseur, S., Grasset, F., and Duguet, E. (2004) Magnetic nanoparticles for medical diagnosis and therapy. *J. Mater. Chem. 14*, 2161−2175.

(5) Weissleder, R., and Papisov, M. (1992) Pharmaceutical iron oxides for MR imaging. *Rev. Magn. Reson. Med. 4*, 1−20.

(6) Weissleder, R., Bogdanov, A., Neuwelt, E. A., and Papisov, M. (1995) Long circulating iron oxides for MR imaging. *Adv. Drug Del. Rev. 16*, 321−334.

(7) Gilchrist, R. K., Medal, R., Shorey, W. D., Hanselman, R. C., Parott, J. C., and Taylor, C. B. (1957) Selective inductive heating of lymph nodes. *Ann. Surg. 146*, 596−606.

(8) van der Zee, J. (2002) Heating the patient: a promising approach? *Ann. Oncol. 13*, 1173−1184.

(9) Hildebrandt, B., Wust, P., Ahlers, O., Dieing, A., Sreenivasa, G., Kerner, T., Felix, R., and Riess, H. (2002) The cellular and molecular basis of hyperthermia. *Crit. Rev. Oncol. Hematol. 43*, 33−56.

(10) Engin, K. (1996) Biological rationale and clinical experience with hyperthermia. *Control. Clin. Trials 17*, 316−342.

(11) Gordon, R. T., Hines, J. R., and Gordon, D. (1979) Intracellular Hyperthermia - A biophysical approach to cancer treatment via intracellular temperature and biphysical alteration. *Med. Hypotheses 5*, 83−102.

(12) Moroz, P., Jones, S. K., and Gray, B. N. (2002) Magnetically mediated hyperthermia: current status and future directions. *Int. J. Hyperthermia 18*, 267−284.

(13) Jordan, A., Scholz, R., Maier-Hauff, K., Johannsen, M., Wust, P., Nadobny, J., Schirra, H., Schmidt, H., Deger, S., Loening, S., Lanksch, W., and Felix, R. (2001) Presentation of a new magnetic field therapy system for the treatment of human solid tumors with magnetic fluid hyperthermia. *J. Magn. Magn. Mater. 225*, 118−126.

(14) Bacri, J. C., Da Silva, M. F., Perzynski, R., Pons, J. N., Roger, J., Sabolovic, D., and Halbreich, A. (1997) *Use of magnetic nanoparticles for thermolysis of cells in a ferrofluid. Scientific and clinical applications of magnetic carriers*. Häfeli, U., Schutt, W., Teller, J., and Zborowski, M., Eds. pp 597−606, Plenum Press, New York.

(15) Jordan, A., Scholz, R., Wust, P., Schirra, H., Schiestel, T., Schmidt, H., and Felix, R. (1999) Endocytosis of dextran and silan-coated magnetite nanoparticles and the effect of intracellular hyperthermia on human mammary carcinoma cells in vitro. *J. Magn. Magn. Mater. 194*, 185−196.

(16) Pitsillides, C. M., Joe, E. K., Wei, X., Anderson, R. R., and Lin, C. P. (2003) Selective cell targeting with light-absorbing microparticles and nanoparticles. *Biophys. J. 84*, 4023−4032.

(17) Mornet, S., Portier, J., and Duguet, E. (2003) Ferrofluides stables en milieu neutre et ferrofluides modifiés obtenus par modification de la surface des particules de ces ferrofluides. French Patent 0306279.

(18) Mornet, S., Portier, J., and Duguet, E. (2005) A method for synthesis and functionalization of ultrasmall superparamagnetic covalent carriers based on maghemite and dextran. *J. Magn. Magn. Mater. 293*, 127−134.

(19) Massart, R. (1982) Magnetic fluids and process for obtaining them. U.S. Patent 4,329,241.

(20) Lee, R. J., and Low, P. S. (1994) Delivery of liposomes into cultured KB cells via folate receptor-mediated endocytosis. *J. Biol. Chem. 295*, 3198−3204.

(21) Lemarchand, C., Couvreur, P., Besnard, M., Costantini, D., and Gref, R. (2003) Novel polyester-polysaccharide nanoparticles. *Pharm. Res. 20*, 1284−1292.

(22) Johnsson, B., Lofas, S., and Lindquist, G. (1991) Immobilization of proteins to a carboxymethyldextran-modified gold surface for biospecific interaction analysis in surface plasmon resonance sensors. *Anal. Biochem. 198*, 268−277.

(23) Antony, A. C. (1992) The biological chemistry of folate receptors. *Blood 79*, 2807−2820.

(24) Gabizon, A., Horowitz, A. T., Goren, D., Tzemach, D., Mandelbaum-Shavit, F., Qazen, M. M., and Zalipsky, S. (1999) Targeting folate receptor with folate linked to extremities of poly(ethylene glycol)-grafted liposomes: in vitro studies. *Bioconjug. Chem. 10*, 289−298.

(25) Sonvico, F., Stella, B., Appel, M., Chacun, H., Marsaud, V., Renoir, M., Colombo, P., and Couvreur, P. Setup of an in

vitro model expressing the folate receptor for the investigation of targeted delivery systems. *J. Drug Delivery Sci. Technol.*, in press.
(26) Carmichael, J., DeGraff, W. G., Gazdar, A. F., Minna, J. D., and Mitchell, J. B. (1987) Evaluation of a tetrazolium-based semiautomated colorimetric assay: assessment of chemosensitivity testing. *Cancer Res. 47*, 936−942.
(27) Salmaso, S., Semenzato, A., Caliceti, P., Hoebeke, J., Sonvico, F., Dubernet, C., and Couvreur, P. (2004) Specific antitumor targetable beta-cyclodextrin-poly(ethylene glycol)-folic acid drug delivery bioconjugate. *Bioconjug. Chem. 15*, 997−1004.
(28) Pinto-Alphandary, H., Balland, O., and Couvreur, P. (1995) A new method to isolate polyalkylcyanoacrylate nanoparticle preparations. *J. Drug Target. 3*, 167−169.
(29) Bootz, A., Vogel, V., Schubert, D., and Kreuter, J. (2004) Comparison of scanning electron microscopy, dynamic light scattering and analytical ultracentrifugation for the sizing of poly(butyl cyanoacrylate) nanoparticles. *Eur. J. Pharm. Biopharm. 57*, 369−375.
(30) Csaba, N., Caamano, P., Sanchez, A., Dominguez, F., and Alonso, M. J. (2005) PLGA: poloxamer and PLGA: poloxamine blend nanoparticles: new carriers for gene delivery. *Biomacromolecules 6*, 271−278.
(31) Petri-Fink, A., Chastellain, M., Juillerat-Jeanneret, L., Ferrari, A., and Hofmann, H. (2005) Development of functionalized superparamagnetic iron oxide nanoparticles for interaction with human cancer cells. *Biomaterials 26*, 2685−2694.
(32) Zhang, Y., Sun, C., Kohler, N., and Zhang, M. (2004) Self-assembled coatings on individual monodisperse magnetite nanoparticles for efficient intracellular uptake. *Biomed. Microdevices 6*, 33−40.
(33) Zhang, Y., Kohler, N., and Zhang, M. (2002) Surface modification of superparamagnetic magnetite nanoparticles and their intracellular uptake. *Biomater. 23*, 1553−1561.
(34) Lemarchand, C., Gref, R., and Couvreur, P. (2004) Polysaccharide-decorated nanoparticles. *Eur. J. Pharm. Biopharm. 58*, 327−341.
(35) Moghimi, S. M., Hunter, A. C., and Murray, J. C. (2001) Long-circulating and target-specific nanoparticles: theory to practice. *Pharmacol. Rev. 53*, 283−318.
(36) Hobbs, S. K., Monsky, W. L., Yuan, F., Roberts, W. G., Griffith, L., Torchilin, V. P., and Jain, R. K. (1998) Regulation of transport pathways in tumor vessels: role of tumor type and microenvironment. *Proc. Natl. Acad. Sci. U.S.A. 95*, 4607−4612.
(37) Gabizon, A. A. (2001) Stealth liposomes and tumor targeting: one step further in the quest for the magic bullet. *Clin. Cancer Res. 7*, 223−225.
(38) Mislick, K. A., Baldeschwieler, J. D., Kayyem, J. F., and Meade, T. J. (1995) Transfection of folate-polylysine DNA complexes: evidence for lysosomal delivery. *Bioconjugate Chem. 6*, 512−515.
(39) Jansen, G., Barr, H., Kathmann, I., Bunni, M. A., Priest, D. G., Noordhuis, P., Peters, G. J., and Assaraf, Y. G. (1999) Multiple mechanisms of resistance to polyglutamatable and lipophilic antifolates in mammalian cells: role of increased folylpolyglutamylation, expanded folate pools, and intralysosomal drug sequestration. *Mol. Pharmacol. 55*, 761−769.

BC050050Z